Investigation on microstructural, anti-corrosion and mechanical properties of doped Zn–Al–SnO$_2$ metal matrix composite coating on mild steel

O.S.I. Fayomi [a,b,*], A.P.I. Popoola [a], V.S. Aigbodion [c]

[a] Department of Chemical, Metallurgical and Materials Engineering, Tshwane University of Technology, P.M.B. X680, Pretoria, South Africa
[b] Department of Mechanical Engineering, Covenant University, P.M.B 1023, Ota, Ogun State, Nigeria
[c] Department of Metallurgical and Materials Engineering, University of Nigeria, Nsukka, Nigeria

ARTICLE INFO

ABSTRACT

In this study, the microstructural, mechanical and anti-corrosion properties of nanocomposite Zn–Al coating containing SnO$_2$ nanoparticles prepared from sulphates electrolyte by electrodeposition on mild steel substrate was investigated. The morphologies of the coating were analysed using SEM/EDS, AFM Raman and X-ray diffraction. The anticorrosion behaviour of the coating prepared with different concentrations of SnO$_2$ (7 and 13 g/L) and potential of (0.3 and 0.5 V) was examined in 3.65% NaCl solution by using linear polarization techniques. The wear and hardness properties of the coatings were performed under accelerated reciprocating dry sliding wear tests and diamond micro-hardness tester respectively. The results obtained showed that the incorporation of SnO$_2$ in the plating bath brings an increase in corrosion resistance and mechanical properties of Zn–Al–SnO$_2$ composite coatings. The SEM images showed a homogeneous grain structure and finer morphology of the coatings. The hardness values was found to improve with the amount of the SnO$_2$ embedded into the Zn–Al metal deposit and effective deposition parameters.

1. Introduction

Nowadays, application of steel in product manufacturing has gained much interest because of its unique properties such as low cost, recyclability and excellent mechanical characteristics. However, low corrosion resistance of this material is the most important problem [1]. One of the most common approaches to overcome this problem is the application of protective coatings to enhance the life span of this material. Zinc is anodic to steel and therefore offers more protection when applied in thin films of 7–15 μm (0.3–0.5 ml) than similar thicknesses of nickel and other cathodic coatings, except in marine environments where it is surpassed by cadmium (which is somewhat less anodic than zinc to iron and steel) [2,3]. When compared to other metals it is relatively in expensive and readily applied in barrel, tank, or continuous plating facilities [4].

Zinc is often preferred for coating iron and steel parts when protection from either atmospheric or indoor corrosion is the primary objective. electroplated zinc without subsequent treatment becomes dull gray in appearance after exposure to air [5]. Bright zinc that has been subsequently given a chromate conversion coating or a coating of clear lacquer (or both) is sometimes used as a decorative finish, such a finish, although less durable than heavy nickel chromium, in many instances offers better corrosion protection than thin coatings of nickel chromium, and at much lower cost [6,7]. Much recent attention has been focused on the development of techniques for electroplating alloys such as zinc–iron, zinc nickel, and zinc–cobalt. The operating parameters and applications of these coatings are very similar to those for unalloyed zinc. There are many efforts by researchers worldwide to developed Zinc alloy coating and Zinc-metallic/non-metallic composites coating that will enhance better properties than ordinary zinc coating, among the research are: Chuen-Chang and Chi-Ming [8] reported on zinc-nickel alloys electrodeposited on steel by pulse current. The electric variables (average current density and pulse cycle) and bath temperature on chemical compositions and grain size of coatings were studied. Zinc nickel alloys electrodeposited on steel were prepared for atmospheric corrosion tests. In addition, the determination of the chemical compositions and the grain size of the Zn–Ni alloy coatings were conducted by scanning electron microscopy (SEM) combined with energy dispersive X-ray spectroscopy (EDS) and scanning probe atomic force microscope (AFM). Furthermore, Tafel

---

* Corresponding author. Department of Chemical, Metallurgical and Materials Engineering, Tshwane University of Technology, P.M.B. X680, Pretoria, South Africa.
E-mail address: ojosundayfayomi3@gmail.com (O.S.I. Fayomi).

plots were employed to evaluate the alloy corrosion behaviour. There results showed that the coating exhibits better properties.

Anju et al. [9] reported on the electrodeposited nickel–phosphorous (Ni–P) alloy coating: an in-depth study of its preparation, properties and structural transitions. Ni–P deposits with a phosphorous content of up to 20% (wt) were obtained on AA6061 substrates by direct current electrodeposition technique from a solution containing nickel sulphate, nickel chloride, phosphorous acid, phosphoric acid and a wetting agent (sodium lauryl sulphate). The effect of various plating parameters like current density, concentration of phosphorous acid, concentration of phosphoric acid and plating temperature on the P content of the coating as well as the rate of deposition was investigated. They observed that the influence of current density on the P content of the deposit is largely dependent on the concentration of phosphorous acid in the plating bath. Composition, surface morphology, microstructure and mechanical properties of the Ni–P deposits were studied using SEM, EDAX, XRD and nanoindentation techniques. Ni–P electrodeposits with low P content in the range of 4–7 wt% of P exhibited superior microhardness of 7.74–8.57 GPa. With increasing P content in the deposit, the structure undergoes transition from crystalline to nanocrystalline and becomes amorphous above 9.14 wt% of P. Ni–P alloys with some selected compositions were subjected to heat treatment at 400 °C for 1 h in a hot air oven and the resulting variation in mechanical properties was studied using nanoindentation technique.

Hamid Reza et al. [10] reported on film formation and anticorrosive behaviour of Zn-ZSM-5 Nano-Sized Zeolite composite coatings. The zinc-Zeolite Socony Mobil-Five nano-particles (Zn-ZSM-5 NPs) composite was prepared and applied successfully as a new coating material to improve the corrosion resistance of steel. The corrosion type and quality of both pure zinc and our new coating material Zn-ZSM-5 NPs were studied using mass loss, impedance and electro-chemical polarization techniques in a sodium chloride solution. Obtained results affirm that Zn-ZSM-5 NPs are non-permeable and their corrosion resistance is higher than the pure zinc. The surface morphology of our newly synthesized coating material Zn-ZSM-5 NPs was investigated using SEM and X-ray diffraction and the smaller grain size was observed in comparison with the pure zinc coating.

Punith Kumar and Venkatesha [11] studied the fabrication of zinc-nano TiO_2 composite films: electrochemical corrosion studies. The composite coating of zinc–TiO_2 was generated successfully on steel from the optimized zinc electroplating bath containing TiO_2 nanoparticles. The composite zinc–TiO_2 coating produced from bath solution with different amount of TiO_2 was tested for their corrosion behaviour by electrochemical studies using polarization and Impedance methods. The TiO_2 incorporated zinc coatings shown better corrosion resistance towards aggressive media when compare to pure zinc coating. The surface structure was examined from their scanning electron microscopic images and X-ray diffraction spectra. The presence of TiO_2 in the coating was confirmed from energy dispersive X-ray diffraction spectra. The embedded TiO_2 nanoparticles changed the compactness, microstructure and preferred orientation of the deposit when compared to pure zinc coating. In this study an attempt to develop compactable and structural modified coating composites that will work against chemical and mechanical deterioration with the help of Zn–Al–SnO_2 metal matrix composite coating on mild steel was studied.

2. Experimental procedure

2.1. Preparation of substrates

Rectangular sectioned flat specimens of commercially sourced mild steel of (40 mm × 20 mm × 1 mm) sheet was used as cathode substrate and 99.5% zinc plate of (30 mm × 20 mm × 1 mm) were prepared as anodes. The initial surface preparation was performed with finer grade of emery paper as described in our pre-

vious studies [12,13]. The sample were properly cleaned with sodium carbonate, pickled and activated with 10% HCl at ambient temperature for 10 s then followed by instant rinsing in deionized water. The mild steel specimens were obtained from metal sample site in Nigeria. The chemical composition of the sectioned sample is shown in Table 1 as obtained from spectrometer analyzer.

2.2. Processed composition

The electrolytic chemical bath of Zn–Al–Sn fabricated alloy was performed in a single cell containing two zinc anode and single cathode electrodes. The distance between the anode and the cathode was 15 mm. Before the plating, All chemical used were analar grade and de-ionized water were used in all solution admixed. The bath was preheated at 40 °C. The processed parameter and bath composition admixed used for the different coating matrix is as follows Zn 75 g/L, Al 30 g/L, K_2SO_4 50 g/L, $ZnSO_4$ 75 g/L, Boric acid 10 g/L, SnO_2 7 g-13 g/L, pH 4.8, time, 20 min and temperature 40 °C. The prepared zinc electrodes were connected to the rectifier at varying applied potential and current density between 0.3 V and 0.5 V at 2 A/cm² for 20 min (see Tables 2 and 3). The distance between the anode and the cathode with the immersion depth were kept constant. The fabricated were rinsed in distilled water and samples air-dried. Portion of the coating were sectioned for characterization.

2.3. Characterization of coating

The structural evolution of the deposited composite coating alloy was characterized with VEGA TESCAN Scanning electron microscope equipped with EDS. The phase change was verified with XRD. Micro-hardness studies were carried out using a Diamond pyramid indenter EMCO Test Dura-scan micro-hardness testers at a load of 10 g for a period of 20 s. The average microhardness trend was measured across the coating interface in an interval of 2 cm using screw gauge attached to the Dura hardness tester.

2.4. Friction and wear tests

The friction and wear properties of the deposited quaternary fabricated alloy were measured using CERT UMT-2 tribological tester at ambient temperature of 25 °C. The reciprocating sliding tests was carried out with a load of 5 N, constant speed of 5 mm/s, displacement amplitude of 2 mm in 20 min. A Si_3N_4 ball (4 mm in diameter, HV50g1600) was chosen as counter body for the evaluation of tribological behaviour of the coated sample. The dimension of the wear specimen was 2 cm by 1.5 cm as prescribed by the specimen holder. After the wear test, the structure of the wear scar and film worn tracks were further examined with the help of high Nikon Optical microscope (OPM) and scanning electron microscope couple with energy dispersive spectroscopy (VEGAS-TESCAN SEM/EDS).

2.5. Electrochemical studies

Linear potentiodynamic polarization tests were carries out on the mild steel deposited composites coating as well as the as-received sample. Measurements were done using an Auto lab potentiostat (PGSTAT30 computer controlled) with the General Purpose Electrochemical Software (GPES) package versions 4.9. Measurements were made at room temperature in 3.65% NaCl solution. The solution for this study was prepared from analytical grade reagents and de-ionised water. An electrochemical cell consisting of working electrode of working electrode (samples) graphite rods as the counter electrodes and a silver chloride 3 M KCl electrode as the reference electrode (SCE). The corrosion potential (E_{Corr}), and corrosion rate were determined accordingly. The specimens were scanned from a potential of −1.5 to + 1.5V.

3. Result and discussion

3.1. SEM/EDS analysis of Zn–Al–SnO_2 sulphates deposited mild steel

The microstructural images of the deposited co-composite fabricated alloy were taken at different matrix to understand the intricacy of particle distribution and morphological enhancement of Zn–Al–SnO_2 sulphates process layers. The typical surface morphology of the composite coating considered for Zn–Al–7Sn–0.3V and Zn–Al–13Sn–0.5V coatings developed are presented in Fig. 1a

Table 1
Chemical composition of mild steel used (wt%).

Element	C	Mn	Si	P	S	Al	Ni	Fe
Composition	0.15	0.45	0.18	0.01	0.031	0.005	0.008	Balance

Table 2
Electrodeposition parameters and results for Zn–Al–SnO$_2$ deposited mild steel.

Sample numbers	Time (min)	Voltage (V)	Additive conc. (g)
Zn–Al–Sn–S	20	0.3	7
Zn–Al–Sn–S	20	0.5	7
Zn–Al–Sn–S	20	0.3	13
Zn–Al–Sn–S	20	0.5	13

Table 3
Summarized data of deposited samples for Zn–Al–SnO$_2$ sulphates bath formulation.

Composition	Mass concentration (g/L)
Zn	75
Al	30
K$_2$SO$_4$	50
Boric acid	10
SnO$_2$	7–13 g
ZnSO$_4$	75
pH	4.8
Voltage	0.3–0.5 V
Time	20 min
Tempt	40 °C

and b From the EDS quantified profile, several primary and few secondary element are identifies. The presence of Sn, Al, and Zn was noticed in all coated deposits. The morphology of Zn–Al–7Sn–0.3V composite coating revealed the dissolution and precipitation of the Al–Sn particle in the zinc-rich matrix interface. The presence and precipitation resulting into compactable crystal seem will be well appreciated by comparing the micrograph of the produced composite coating at 13 g/L in 0.5 V (see Fig. 2a and b).

The micrograph in Fig. 1b of the Zn–Al–13Sn–0.5V coatings reveals a reduced crystal grain and precipitate fully covering the surface at the particle-matrix interfaces. This structural properties form might be as a result of the interfacial particle relation at the moderate level participating in adsorption, the nucleation part exposed by zinc-rich matrix and the bonding energy in term of applied potential. Similar properties of established morphology at the interface was reported by Sancakoglu et al. [7]. However, it can be inferred that the embedded SnO$_2$ particle incorporated is highly dependent on the stable dispersion of the particulate in the bath otherwise severe segregation and non-uniform distribution could have be seen and this is supported by Dong et al. [14].

3.2. Atomic force microscope (Zn–Al–SnO$_2$ deposition)

AFM photomicrographs obtained from the Zn–Al–SnO$_2$ sulphates composite coatings on mild steel are shown in Fig. 3. Comparing these micrographs at different value of additive incor-

poration of 7 g/L and 13 g/L in altered applied potential from 0.3 V to 0.5 V respectively, it was observed that the Zn–Al–13SnO$_2$ at 0.5V sulphates coating (see Fig. 3) shows a perfect distribution of Al/Sn intermetallic particles with uniform grains and crystal size. The effect of the perfect growth and nodule form can be described in term of deposition kinetics of ion diffusion in relation to the volume of particulate in the bath and also charge transfer reaction which is proportional to the diffusion and growth rate Mohankumar et al. [3].

The compartment and adhesion of the Zn–Al–13SnO$_2$ at 0.5 V as against Zn–Al–7SnO$_2$ −0.3V in Fig. 3 indicate that increase coating thickness is not proportional to the quality of adhesion as against the report by Abou-Krisha et al. [15] that the surface roughness increases significantly with the film thickness. Invariably such condition is not valid in all case as observed in this study. Though, particle infringement could results in crystal build up. [16], adhesion, perfect dispersion and topography are function of exact process parameter especially the applied voltage or current [17]. More so, it is noteworthy to mention that refining of the crystallites took place with accurate throwing power exerted which should lead give coalesced crystallites as observed in Fig. 3. The interfacial phases such as SnAlZn$_2$ and Sn$_2$Al$_2$Zn$_2$ in Zn–Al coating possibly led to the formation of more densely packed deposits.

In general, high refinement of crystal growth and uniform arrangement of the distributed crystals was achieved more in Fig. 4 which is in line with the Yang et al. [6] opinion on ternary coating fabrication.

3.3. Solid XRD analysis of Zn–Al–SnO$_2$ sulphates deposited mild steel

The XRD patterns of co-deposited layers of Zn–Al–7SnO$_2$–0.3Vand Zn–Al–13SnO$_2$–0.5V on steel are presented in Figs. 4 and 5 respectively. In the quantified phase performed for Zn–Al–7SnO$_2$–0.3V composite coating, Zn, Al, Al$_3$Zn, Sn$_2$Zn$_3$; and Zn$_3$Sn phases were identified in the coating matrix (Fig. 4). For deposit obtained for Zn–Al–13SnO$_2$–0.5V, a more crystalline and possible reactions that resulted into phases are Zn, Zn$_2$AlSn, Zn$_3$Sn, Zn$_3$Sn$_2$; and Zn$_7$Sn. The given composition of the surface layers was assessed and all the samples showed higher peak spectra as against the formal. Taking a good study of the recorded phase there are four intermetallic phases together with the main constituent Zn.

The elemental Al and Sn peak does not observed to exist as single phase indicating that the proportion of the admixed composite particulate and the activities reacted homogeneously to form an in-situ phase presented. The unique existence of Zn at the interfacial surface of the deposit as a single peak is as a result of profusion of zinc within the bath. The main peaks for the ZnSn phase occur at $2\theta = (45.12°, 55.10°$ and $70.22°)$. The zinc rich exist within $2\theta = (38.22°, 39.98°,$ and $68.2°)$. More so, unique broad phase consistence three intermetallic deposit were notice at $2\theta = (38.50°)$ for Zn$_2$AlSn. With this phases a proof of complete dissolution of the
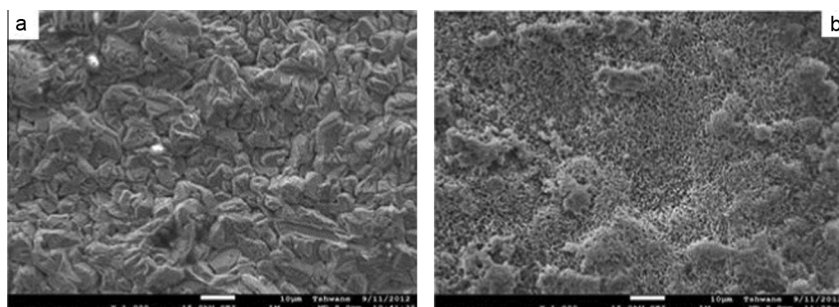

Fig. 1. SEM/EDS showing the surface morphology of (a) Zn–Al–7Sn–0.3V (b) Zn–Al–13Sn–0.5V sulphates deposited sample.
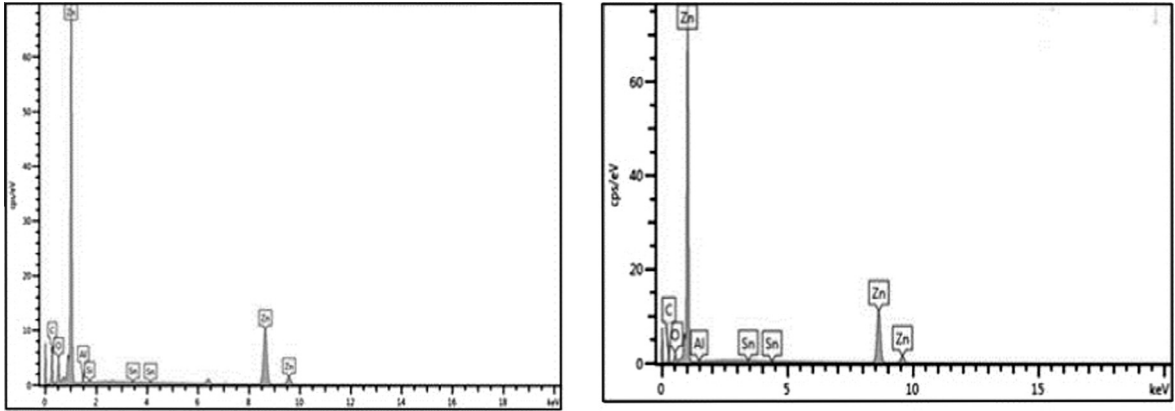
Fig. 2. EDS showing the surface morphology of (a) Zn–Al–7Sn–0.3V (b) Zn–Al–13Sn–0.5V sulphates deposited sample.
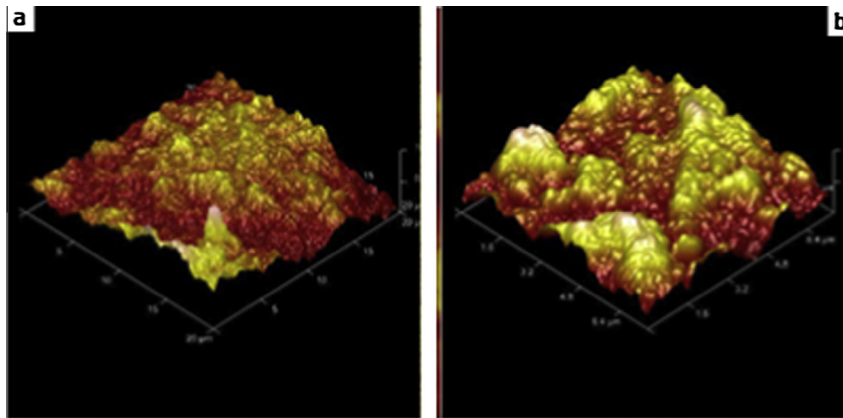

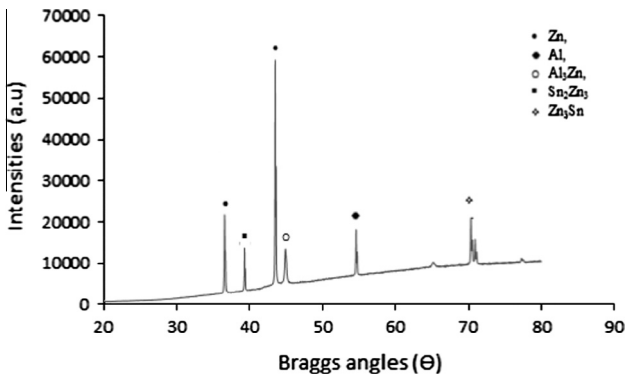Fig. 3. AFM images of the (a) Zn–Al–7Sn–S–0.3V (b) Zn–Al–13Sn–S–0.5V.

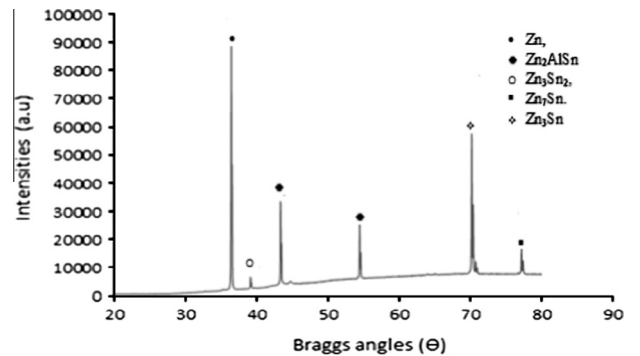Fig. 4. Solid X-ray diffraction profile for Zn–Al–7Sn–0.3V.

Fig. 5. Solid X-ray diffraction profile for Zn–Al–13Sn–0.5V.

composite particulate as against the formal with Al at the interface. In the other hand, some of the phases with peaks of Zn_2AlSn are anticipated to enhance the build-up of strong intermetallic precipitates thereby producing fine grain microstructures. The difference in their peak level affirms the bonding effect of Zn–Al–13SnO_2–0.5V (see Fig. 5) as against Zn–Al–7SnO_2–0.3V phase.

3.4. Micro-hardness analysis of Zn–Al–SnO$_2$ sulphates deposited mild steel

The micro-hardness (HVN) value of the deposited composite coatings for each sample at different applied potential was measured. Fig. 6, showed the average micro-hardness data for the Zn–Al–SnO$_2$ sulphates deposits at different matrixes. It can be seen from Fig. 6 that hardness increased for all composite layer ranging from approximately 34 HVN for base mild steel to approximately 202 HVN for highest value obtained of the co-deposited series.

The catalytic activities that lead to improvement of the Zn–Al–SnO$_2$ especially for the best improved coating (Zn–Al–13Sn–0.5V) alloy are attributed to the sufficient presence of SnO$_2$ that enhance Zn^{2+}/Al^{3+}. Although, the Zn^{2+} ion help in nucleation, but the presence of Al^{3+} and SnO$_2$ are considered the main effect and intermediaries for reduced Zn particle size and increase the actual surface area for prefer morphology which guarantees improved hardness at all deposited composite coating parameter. To justify the effect
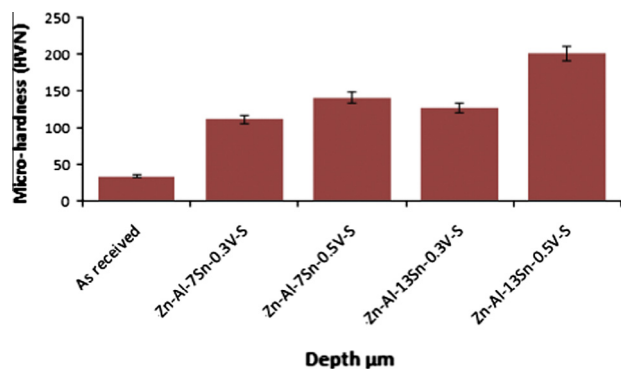
Fig. 6. The microhardness/depth profile for Zn–Al–Sn sulphates deposited sample.

Fig. 7. Variation of the wear loss with time of Zn–Al–Sn–S.

of composite-particle introduce i.e. SnO_2 in Zn/Al interface, the composite particles are increase and the plating condition (applied voltage) likewise were also increased. However it is a known fact that bath composition and plating potential defined a kind of surface modification which is proportional to the improvement of hardness properties that was expected, this is in par with the work of Abdel et al. [18].

In another report, bath content and process parameter have been attested to influence the nature of deposit produce thereby absorbing on the electrode surface which in turn possess significant role in buildup of morphology and interfacial characteristics [17]. The acclaim ideal by the authors is in conformity with the result obtained. In essence, the volume of wt% of particulate admixed in bath increase as the hardness behaviour increase. The degree of energy expended (applied potential) also could be seen to affect positively the hardness properties. It is also important to state that adhesive properties are function of exact precipitation of solid solution in the bath. This precipitate on substrate defines the nature of crystal. This is in line with supported report by Popoola et al. [12] and Subramanian et al [19] that higher hardness of the coating are often determine by fine-grained structure of the deposit and the dispersed volume of introduce particles in the fine-grained matrix which may obstruct the easy movement of dislocations, to give a higher mechanical properties.

3.5. Wear rate evaluation of Zn–Al–SnO₂ sulphates deposited mild steel

The wear properties of Zn–Al–SnO_2 sulphates composite coating samples was carried out and presented in Fig. 7. The graphs of the variation of the wear mass loss are a function of time for all composite fabricated coating and mild steel respectively. As can be seen the wear loss attained for all composite fabricated coating are very minimal with range between 0.003 and 0.005 g/min as compare to plough deformation by the control sample of about 2.351 g/min. The addition of admixed metal matrix composite to the substrate by the co-deposition techniques improved the overall anti-wear properties significantly. The Zn-Al-13Sn–0.5V matrix gave the best wear resistance with over 100% maximal reduction in wear rate, signifying the lowest mass loss within the composite-fabricated group. This phenomenon in co-deposition of composite are often attributed to the strong activities of the particle embedded [16] and the process condition for the fabrication of the such composite coating [18].

Basically SnO_2 may not have tremendously be known as hard material as compare to major ceramics but its interfacial bonding force with Zn/Al could be seen to provide a strong interface and reinforcement phase which is beneficial to the wear resistance observed for all coated alloy. It is important to mention that only
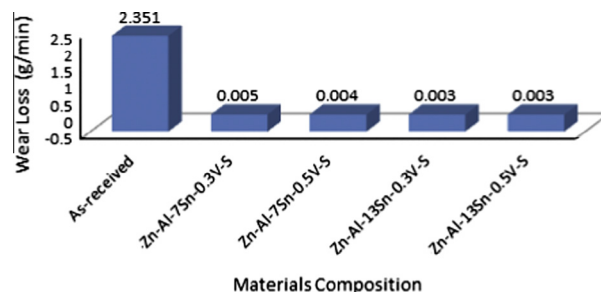
slight differences are notice among the mass loss of the Tin-metal matrix which may be due to the compositional variation and the morphological properties attained from process parameter.

The as-received substrate, deposited Zn–Al–7Sn–0.3V and Zn–Al–13Sn–0.5V coatings was subjected to wear testing with wear track shown in Fig. 8 respectively. The wear scar of the substrate (Fig. 8) shows very deep pits, large groves and pronounced debris on the material surface. The wear track of the co-deposited composite coatings Fig. 8a–c for Zn–Al–7Sn–0.3V and Zn–Al–13Sn–0.5V respectively presented wear scar morphology with less debris.

Invariably the combined interfacial effect of the Zn/Al and Sn most especially for Zn–Al–13Sn–0.5V coating produced a strong phase as in-situ. This in-situ bond between the admixed produced coatings has stronger influence, and exhibit wear resistance properties than other coatings. More so, it is necessary to note and ascertain the essence of fraction of embedded composite as it relate to progression of anti-wear characteristics. One might expect that beyond 7 g/L, cluster of the particle will increase in the electrolyte thereby making the time for embedment in to zinc–metal matrix longer and hence cause detriment to grain structure and as a result accelerate excessive fracture and damages of the coated layer. In this work, the situation seem different as particle incorporated at sulphates processing support the precipitation, reduce crystal size and promote wear resistance.

3.6. Electrochemical result of Zn–Al–SnO₂ composite

The potentiodynamic polarization curves of the as-received and composite coating specimens in 3.65% NaCl solution at 25 °C are shown in Fig. 9. The pitting potentials, the corrosion current densities and the polarization potentials of all the fabricated composite coating are obtained from polarization curve presented in Table 4. It can be seen in Fig. 9 that the anodic and cathodic process of all the composite fabricated layer is significantly surprised, indicating a higher corrosion potential and lower current densities' as compare to the as-received metal.

The best among the fabricated alloy which is Zn–Al–13Sn–0.5V showed passivity with corrosion potential of −1.05042 V, a three orders improvement in magnitude as against the mild steel substrate of −1.53900 V. The least potential of the composite coating is −1.19781 V for Zn–Al–7Sn–0.3V–S. The results of this coatings although is envisage with various fact (1) since microstructural studies revealed a reasonable uniform distribution as a results of SnO_2 in the Zn/Al blend, solid intermediate phase that will overcome porous formation are attain which retard the penetration of chloride ion infringement. (2) Uniform particle incorporation within the lattices in the metallic deposit could decrease the active surface in contact with oxidation environment thereby enhancing the polarization resistance.

In note shell, the corrosion rate decreases from 4.1 mm/yr. of as-received sample to 0.002954 mm/yr. for Zn–Al–13Sn–0.5V best
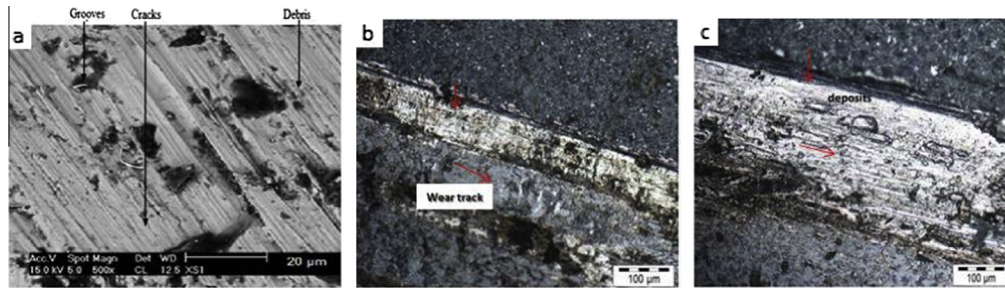
Fig. 8. Micrograph of the wear scar for (a) mild steel (b) Zn–Al–7Sn (c) Zn–Al–13Sn sulphates deposited sample.
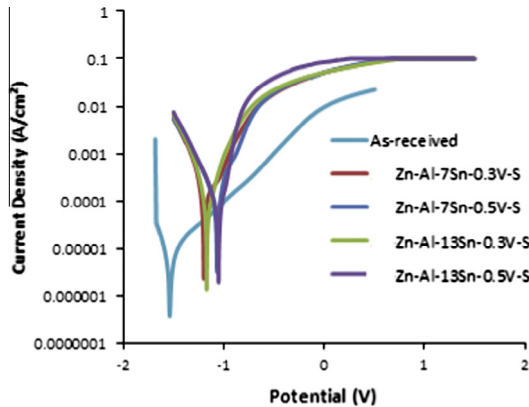

Fig. 9. Potentiodynamic polarization curves for Zn–Al–Sn sulphates deposited mild steel.

composite coating among the group owing to the buildup of strong adhesive films. In general, this phenomenon implies that the presence of Al/Sn oxide content in the deposited alloy strongly increases the corrosion resistance of the coatings.

The sequence of polarization resistance (R_p) in a decreasing trend follows 32-Zn–Al–13Sn–0.5V–S > 30–Zn–Al–7Sn–0.5V–S > 31–Zn–Al–13Sn–0.3V–S > 29–Zn–Al–7Sn–0.3V–S and As-received

with identify value as 724.38 Ω > 649.52 Ω > 565.53 Ω > 541.91 and 27.600 Ω respectively.

The anti-corrosion ability of the composite coating was examined with OPM studies. The results of the corrosion interference are presented in Fig. 10a and b respectively. For deposit produce with 13 g/L at 0.5 V. Fig. 10b, the chloride intrusion into the interface was not noticed since morphological change are associated to strong blocking effect, the result of the nuclei proportion owning to needle growth, volume of particle embedment may be a major force behind the dictate of retardation and unseen pits. Another interesting relationship for corrosion damage resistance in line with the results obtained is the report by Rahman et al. [4] that the morphological characteristics of deposited coating depend on the applied voltage, bath composition and the additives. Praven and Venkatashe [13] said since the deposition rate is slow at low applied voltage, at the beginning of the electrolysis, alloy deposits has a large number of tiny particles on almost all over the cathode surface which acts as nucleation for further deposition at the preferential sites.

In view of this, resistance to failure of Zn–Al–13Sn–0.5V–S was as results of better morphology and good adhesion stability. For Zn–Al–7Sn–0.3V sulphates the situations were bit difference. The chloride ion aggressively fine way into the intermediate bond of the matrix which later form oxide inform of corrosion product on the surface. Pit within the interface were also noticed.

Table 4
Summary of the potentiodynamic polarization results of Zn–Al–Sn.

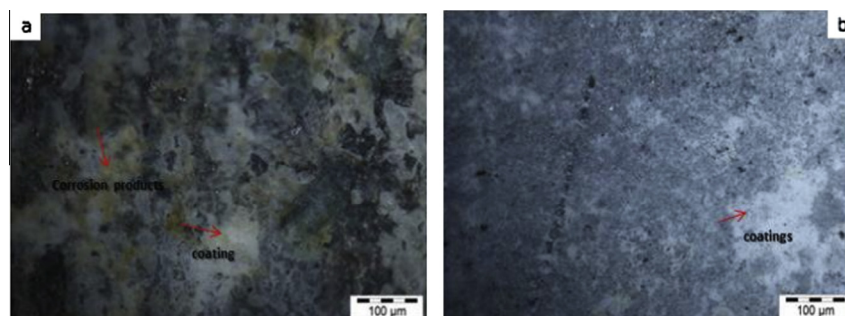| Sample No.	I_{corr} (A/cm^2)	R_P (Ω)	E_{corr} (V)	Corrosion rate (mm/yr)
As-received	7.04E−02	27.600	−1.53900	4.100000
Zn–Al–7Sn–0.3V–S	1.91E−05	541.91	−1.19781	0.222180
Zn–Al–7Sn–0.5V–S	1.42E−05	649.52	−1.06689	0.005941
Zn–Al–13Sn–0.3V–S	1.89E−05	565.53	−1.16943	0.007887
Zn–Al–13Sn–0.5V–S	7.08E−06	724.38	−1.05042	0.002954

Fig. 10. Morphology of (a) Zn–Al–7Sn–0.3V sulphates (b) Zn–Al–13Sn–0.5V sulphates deposited mild steel after corrosion.

4. Conclusions

From the results and discussion above the following conclusions can be made:

1. Morphological evolution of the Zn–Al–SnO$_2$ sulphates composite coating by co-deposition matrix has successfully been achieved from different matrix.
2. The microstructure produced consists intermetallic phase of Zn, Zn$_2$AlSn, Zn$_3$Sn, Zn$_3$Sn$_2$; and Zn$_7$Sn which are prominent to improvement of the hardness and wear resistance properties.
3. The highest wear resistance was produced among the matrix composite was 0.003 g/min for Zn–Al–13SnO$_2$–0.5V as against 2.351 g/min for base mild steel.
4. The highest hardness produced among the matrix composite was 202 HVN for Zn–Al–13SnO$_2$–0.5V as against 34 HVN for base mild steel.
5. The electrochemical study revealed good anti-corrosion resistance properties was attained for the deposited alloy as a result of solid precipitation of zinc–aluminum–tin deposition. The sample produced with the highest applied potential deposition; highest particle incorporation provides a wild spread of potential protection.

Acknowledgement

References

[1] O.S.I. Fayomi, M. Abdulwahab, A.P.I. Popoola, Properties evaluation of ternary surfactant-induced Zn–Ni–Al$_2$O$_3$ films on mild steel by electrolytic chemical deposition, J. Ovonic Res. 9 (5) (2013) 123.
[2] R.E. Melchers, B.B. Chernov, Corrosion loss of mild steel in high temperature hard freshwater, J. Corros. Sci. 52 (2010) 449.
[3] C. Mohankumar, K. Praveen, V. Venkatesha, K. Vathsala, O. Nayana, Electrodeposition and corrosion behavior of Zn–Ni and Zn–Ni–Fe$_2$O$_3$ coatings, J. Coat. Technol. Res. 9 (1) (2012) 71–77.
[4] M.J. Rahman, S.R. Sen, M. Moniruzzaman, K.M. Shorowordi, Morphology and properties of electrodeposited Zn–Ni alloy coatings on mild steel, J. Mech. Eng., Trans. Mech. Eng. Div., Inst. Eng., Bangladesh 40 (1) (2009) 9–12.
[5] R. Xu, J. Wang, Z. Guo, H. Wang, Effect of rare earth on microstructures and properties of Ni–W–P–CeO$_2$–SiO$_2$ nano-composite coating, J. Rare Earth 26 (4) (2008) 579–583.
[6] G. Yang, S. Chai, X. Xiong, S. Zhang, L. Yu, P. Zhang, Preparations and tribological properties of surface modified Cu nanoparticles, Trans. Non Ferrous Metals Soc. China 22 (6) (2012) 366.
[7] O. Sancakoglu, O. Culha, M. Toparli, B. Agaday, E. Celik, Co-deposited Zn-submicron sized Al$_2$O$_3$ composite coatings: production, characterization and micromechanical properties, J. Mater. Des. 32 (3) (2011) 4054.
[8] Chuen-Chang, H. Chi.-Ming, Zinc–nickel alloy coatings electrodeposition by pulse current and their corrosion behavior, J. Coat. Technol. Res. 3 (2) (2006) 99.
[9] Anju M. Pillai, A. Rajendra, A.K. Sharma, Electrodeposited nickel–phosphorous (Ni–P) alloy coating: an in-depth study of its preparation, properties, and structural transitions, J. Coat. Technol. Res.. 9 (6) (November 2012) 785–797.
[10] Hamid Reza Safaei, Mohammad Reza Safaei, Vahid Rahmanian, Film formation and anticorrosive behavior of Zn–ZSM-5 nano-sized zeolite composite coatings, Open Electrochem. J. 4 (2012) 1–8.
[11] M.K. Punith Kumar, T.V. Venkatesha, Fabrication of zinc-nano TiO$_2$ composite films: electrochemical corrosion studies, J. Chem. Pharm. Res. 5 (5) (2013) 253–261.
[12] A.P.I. Popoola, O.S.I. Fayomi, O.M. Popoola, comparative studies of microstructural, tribological and corrosion properties of plated Zn and Zn-alloy coatings, Int. J. Electrochem. Sci. 7 (9) (2012) 4860.
[13] B.M. Praveen, T.V. Venkatesha, Electrodeposition and properties of Zn-nanosized TiO$_2$ composite coatings, Appl. Surf. Sci. 254 (8) (2008) 2418.
[14] D. Dong, X.H. Chen, W.T. Xiao, G.B. Yang, P.Y. Zhang, Preparation and properties of electroless Ni–P–SiO$_2$ composite coatings, Appl. Surf. Sci. 255 (5) (2009) 7051.
[15] M.M. Abou-Krisha, F.H. Assaf, S.A. El-Naby, Electrodeposition behavior of zinc–nickel–iron alloys from sulfate bath, J. Res., Coat. Technol. 6 (3) (2009) 391–399.
[16] A. Gomes, T. Frade, I.D. Nogueira, Morphological characterization of Zn-based nanostructured thin films, Curr. Microsc. Contribut. Adv. Sci. Technol. 2 (1) (2012) 1146.
[17] T.G. Wang, D. Jeong, Y. Liu, S. Lyengar, S. Melin, K.H. Kim, Study on nanocrystalline Cr$_2$O$_3$ films deposited by arc ion plating: II. mechanical and tribological properties, J. Surf. Coat. Technol. 206 (10) (2012) 2638.
[18] A.A. Abdel, H.B. Hassan, M.A. Abdel Rahim, Nanostructured Ni–P–TiO$_2$ composite coatings for electrocatalytic oxidation of small organic molecule, J. Electroanal. Chem. 620 (2008) 17.
[19] B. Subramanian, S. Mohan, S. Jayakrishnan, Structural, microstructural and corrosion properties of brush plated copper-tin alloy coatings, Surf. Coat. Technol. 201 (7) (2006) 1145.